From Fully Stretched to Collapsed Chains: Bottlebrush Polymer Grafted Particles

Jensen N. Sevening,[a] Nehal Nupnar,[b] Soumyanil Adhikary,[c] Danielle Reifsnyder Hickey,[a,c,d] Matthew T. Swulius,[e] Hilmar Koerner,[f] Michael J. A. Hore,[b] Robert J. Hickey[a,d*]

[a]Department of Materials Science and Engineering, The Pennsylvania State University, University Park, PA 16802, USA

[b]Department of Macromolecular Science and Engineering, Case Western Reserve University, Cleveland, OH 44106, USA

[c]Department of Chemistry, The Pennsylvania State University, University Park, PA 16802, USA

[d]Materials Research Institute, The Pennsylvania State University, University Park, PA 16802, USA

[e]Department of Biochemistry and Molecular Biology, Penn State Hershey College of Medicine, Hershey, PA 17033, USA

[f]Materials & Manufacturing Directorate, Air Force Research Laboratory, Wright-Patterson AFB, OH 45433 USA

*Corresponding author: rjh64@psu.edu

Abstract

Macromolecular architecture is a critical parameter when tuning polymer material properties. Although the implementation of non-linear polymers in different applications has grown over the years, polymer grafted surfaces such as nanoparticles have traditionally been composed of linear thermoplastic polymers, with a limited number of examples demonstrating a diversity in polymer architectures. In an effort to combine polymer architecturally dependent material properties with polymer grafted particles (PGPs), as opposed to conventional methods of tuning polymer grafting parameters such as the number of chains per surface area (i.e., polymer graft density), a series of bottlebrush grafted particles were synthesized using surface-initiated ring-opening metathesis polymerization (SI-ROMP). These bottlebrush PGPs are composed of glassy, semi-crystalline, and elastomeric polymer side chains with controlled backbone degrees of polymerization (N_{bb}) at relatively constant polymer graft density on the surface of silica particles with diameters equaling approximately 160 or 77 nm. Bottlebrush polymer chain conformations, evaluated by measuring the brush height of surface grafted polymer chains in solution and the melt, undergo drastic changes in macromolecular dimensions in different environments. In solution, brush heights increase linearly as a function of N_{bb}, consistent with fully stretched chains, which is confirmed using cryogenic transmission electron microscopy (Cryo-TEM). Meanwhile, brush heights are consistently at a minimum in the melt, indicative of chains collapsed on the particle surface. The conformational extremes for grafted bottlebrush polymers are unseen in any linear polymer chain systems, highlighting the effect of macromolecular architecture and surface grafting. Bottlebrush grafted particles are an exciting class of materials where diversifying polymer architectures will expand PGP material design rules that harness macromolecular architecture to dictate properties.

TOC

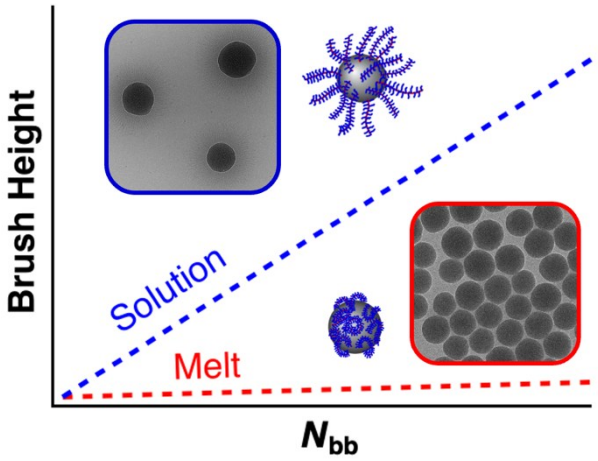

Introduction

Hybrid polymer-inorganic materials simultaneously combine drastically different physical properties into a single material while potentially leading to emergent properties due to synergistic effects.[1–6] A critical factor for successful hybridization of polymers and inorganic components for advanced materials requires controlled filler dispersion, yet traditional mixing methods typically lead to macrophase separation of the differing components, resulting in undesirable and unfavorable properties.[7] A solution for hybrid polymer-inorganic material structural tunability and preventing macrophase separation is the use of polymer grafted nanoparticles (PGNs). The covalently bound chains on the nanoparticle surfaces help to mitigate the thermodynamic driving force for macrophase separation in blended systems. For example, synthetic manipulation of polymer molecular weight and graft density allow for access of nanoparticle sheets, strings, and well-dispersed particles,[8,9] influencing the mechanical,[10–12] optical,[13,14] electrical,[15,16] and magnetic[17] properties. Although there has been significant progress in creating materials containing polymer grafted nanoparticles over the years, the vast field of PGN research has been limited in scope, primarily focusing on linear amorphous thermoplastic polymers. Thus, expanding the diversity of polymer architectures grafted to PGNs will advance material design rules for dictating new properties.

There are two primary approaches for synthesizing PGNs: graft-to and graft-from.[18–20] Both methods have advantages, but graft-from approaches enable independent control of graft density and graft molecular weight, which is critical for tailoring nanoparticle organization. Furthermore, controlled radical polymerizations such as surface-initiated atom transfer radical polymerization (SI-ATRP) and surface-initiated reverse addition-fragmentation chain-transfer (SI-RAFT) have broadened the scope of available polymer chemical compositions.[10,12,21] While the

benefits of expanding the possibilities of different polymer compositions afforded by surface-initiated controlled radical polymerizations are apparent, overwhelmingly many of the PGN examples consist of linear amorphous thermoplastic polymers, which are only a subset of commercially available polymers that encompass semi-crystalline and non-linear polyolefins. Recently, olefin metathesis polymerizations to synthesize poly(norbornene) and poly(cyclooctadiene) have been utilized, including surface-initiated ring-opening metathesis polymerization (SI-ROMP),[22–25] which has unlocked new possibilities for PGN materials exhibiting semi-crystalline[26,27] and softer rubbery properties.[28] An added benefit of SI-ROMP is the access to bottlebrush PGNs,[29–31] which expands the opportunities for exploring nanoparticles grafted with non-linear macromolecular architectures.

Bottlebrush polymers are a class of non-linear macromolecules where a linear backbone is densely grafted with polymer side chains,[32,33] resulting in exceptionally soft polymer materials due to the increase in the entanglement molecular weight.[34] Furthermore, the mechanical properties of bottlebrush polymer materials are dependent on three parameters: backbone degree of polymerization (N_{bb}), side chain degree of polymerization (N_{sc}), and degree of polymerization between side chains (N_g), allowing for enhanced tunability as compared to linear polymers (**Figure 1a**). The versatility in controlling bottlebrush polymer materials through synthetic parameters has led to uses in applications related to tissue-mimicking elastomers,[35,36] photonic crystals,[37,38] batteries,[39] triboelectric nanogenerators,[40] and dielectric elastomer actuators.[41] This work features bottlebrush side chain chemistries of poly(dimethyl siloxane) (PDMS), used in elastomers,[35,42] poly(ethylene oxide) (PEO), used for biocompatibility[36] and drug delivery,[43,44] and poly(styrene) (PS), as a representative glassy polymer.

Additionally, bottlebrushes are known for rapid, highly ordered self-assembled structures,[45,46] which has garnered interest in the field of hybrid materials. Integration of nanoparticles with copolymer bottlebrushes enables directed dispersion of NPs within specific polymer domains,[47–49] yet there are still thermodynamic mixing barriers that lead to macrophase separation of the individual components. Thus, covalently bound bottlebrushes grafted to nanoparticles remain uniquely suited to controlling nanoparticle dispersion. Further, single-component capabilities of PGNs afford simplicity in material processing and recycling. Controlling material ordering and ensuing properties through macromolecular architecture is an intriguing strategy that has thus far been minimally explored for PGNs.[50]

A critical factor for controlling PGN self-assembly is polymer brush dimensions, which directly influences particle assembly and dispersion in PGN systems,[9,50] but has yet to be determined for bottlebrush polymers grafted to nanoparticle surfaces under different conditions. Most research on bottlebrush polymer grafts has focused on planar surfaces, examining how graft density affects conformation. Low graft density allows for a more flexible backbone with side chains extending perpendicularly, whereas high graft density results in a more rigid, elongated backbone with side chains oriented parallel to it.[51,52] The brush conformation may deviate slightly from this pattern when considering adsorption[53] or charge[54] effects. Despite these insights, the existing theoretical and computational studies lack experimental support, especially when varied surface geometries are involved.

Here, we reveal that bottlebrush chain conformations undergo drastic changes depending on whether they are in solution or the melt state. In this study, the bottlebrushes are grafted to large silica nanoparticles (diameter, $d \approx 160$ nm) and will be referred to as polymer grafted particles (PGPs). A series of bottlebrush PGPs with varying chemical compositions and N_{bb} were

synthesized *via* SI-ROMP of macromonomers, bottlebrush graft-through method, and the bottlebrush polymer brush height was characterized under different conditions. The bottlebrush chains are found to be fully stretched in solution and completely collapsed in the melt, which is in striking contrast to the predicted linear chain conformations at the same molecular weight and grafting density. However, there are differences between reported linear chain PGNs and the PGPs here that include lower surface curvature and polymer volume fractions. Combining macromolecular architecture and PGPs has the potential to unlock exciting opportunities in hybrid material design through bottlebrush polymer molecular parameters, chemical composition, and inorganic component functionality (**Figure 1b**).[29,55–61]

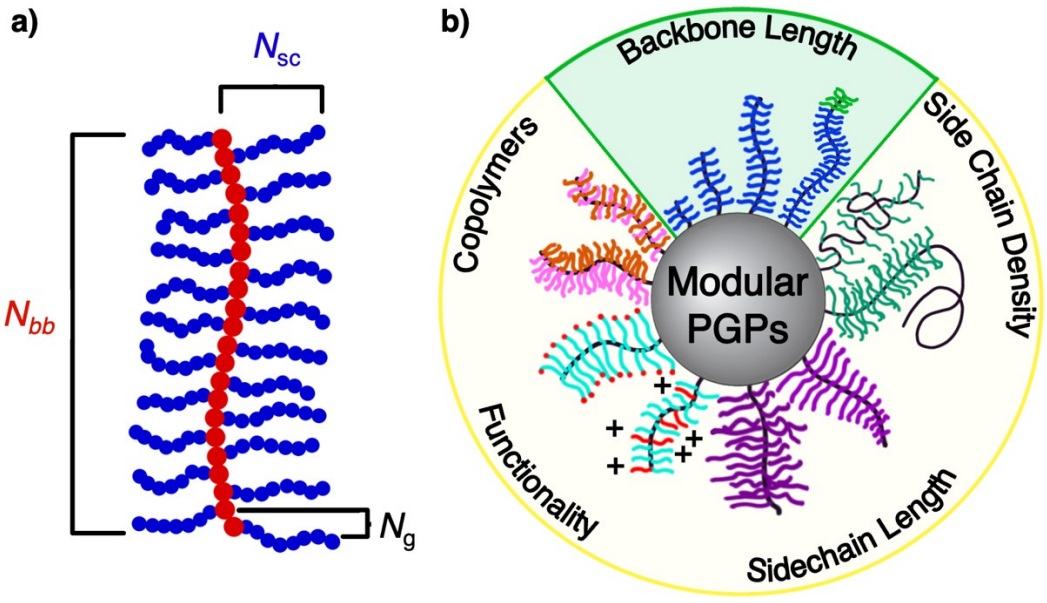

Figure 1. Scheme depicting bottlebrush parameters and modularity afforded to bottlebrush PGPs. (a) Bottlebrush architecture with tunable parameters: backbone degree of polymerization (N_{bb}, red), side chain degree of polymerization (N_{sc}, blue), and degree of polymerization between side chains (N_g). (b) The work reported here examines the effect of backbone length (N_{bb}, green

background) on bottlebrush PGP materials. Polymer synthetic versatility allows for tailored side chain density, side chain length, chemical functionality, or copolymers (yellow background), expanding application possibilities.

Results & Discussion

Synthesis of Bottlebrush PGPs

A series of bottlebrush PGPs with varying N_{bb} were synthesized using a modified SI-ROMP method (**Figure 2a**).[22] First, macromonomers of PS, PEO and PDMS were functionalized with a norbornene end group. The macromonomers were chosen due to differences in glass transition temperature (e.g., PDMS and PS) and crystallization behavior (e.g., PEO). Next, silica particles synthesized using the Stöber method with a diameter of 159 ± 4 nm were surface functionalized with norbornenyltriethoxysilane.[25,62] The norbornene groups on the surface of the particles provide initiation points from which the bottlebrushes are polymerized. The large diameter was utilized for the ability to separate PGPs from homopolymer *via* centrifugation after the reaction. To begin the polymerization, the norbornenyl-functionalized particles were "activated" by adding Grubbs' 3rd generation catalyst (G3) in excess to bind the catalyst with the particle surface and prevent particle coupling.[22,23] The surface-initiated polymerization was started by adding the "activated" particles to macromonomer solutions. The grafted bottlebrush polymers were formed by a combination of 1) the graft-from method (polymer grafted "from" particle) in which the norbornene end-group of the macromonomers ring-open from the particle surface and 2) the graft-through method (bottlebrush polymer grafted "through" its backbone) in which the norbornene ring-opening forms the bottlebrush backbone, resulting in PS, PEO, or PDMS bottlebrush side chains (**Figure 2b-d**).

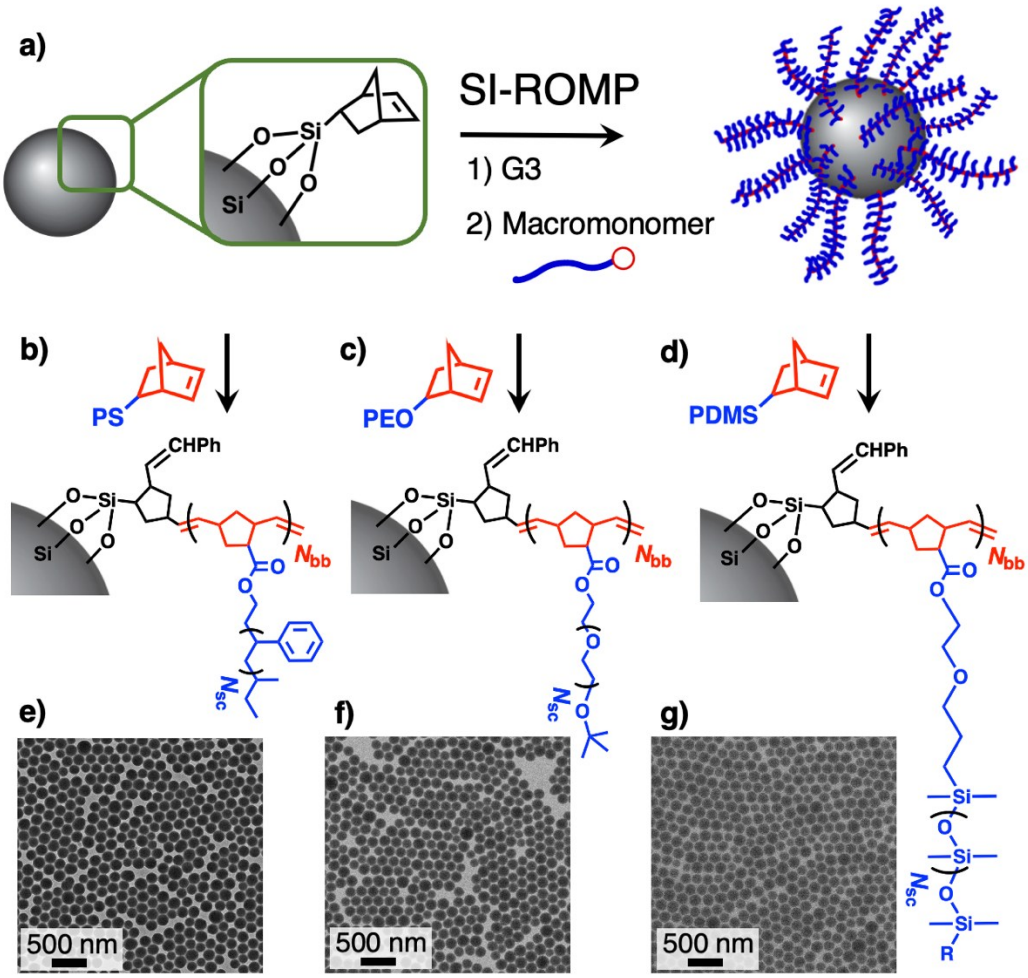

Figure 2. Synthetic overview of bottlebrush PGPs *via* SI-ROMP. (a) Bottlebrush PGPs are synthesized in a two-step method in which the norbornyl silane groups are first "activated" with the G3 catalyst and then the particles are added to norbornene functionalized macromonomers. The bottlebrush polymers have a poly(norbornene) backbone containing three different side chains: (b) PS, (c) PEO, and (d) PDMS. The R group on the PDMS denotes either a methyl or butyl alkane. TEM micrographs of bottlebrush PGPs containing (e) PS, (f) PEO, and (g) PDMS side chains.

The work reported here explores the impact of N_{bb}, as opposed to the two other tunable parameters known to impact bottlebrush polymer material properties, N_{sc} and N_g. N_{sc} and N_g are consistent for PS, PEO, and PDMS samples. The N_{sc} are listed in **Table 1** and N_g is 1, as every repeat unit has a side chain. N_{bb} was controlled by adjusting the reactant ratios of activated particle (e.g., 500 mg) to macromonomer (e.g., 100 mg to 1 g). All reactions were stirred at 40 ˚C for 40 min and terminated with ethyl vinyl ether (EVE). The resulting products were purified through centrifugation (10,000 rpm, 15 min) and resuspension of the PGP pellet in tetrahydrofuran (THF) at least three times. Decanting the supernatant removes catalyst, excess EVE, unreacted macromonomer, and any free homopolymer. A final "light" centrifugation (2,500 rpm, 3 min) separated any large particle aggregations, and the PGP supernatant solution is conserved. Bottlebrush polymer N_{bb} was measured by cleaving the polymers from the particle surface using hydrofluoric (HF) acid, drying the polymer sample, and then conducting size exclusion chromatography (SEC).

The molecular weights of the PS bottlebrush samples were measured *via* SEC using THF as the mobile phase and were found to be 139, 327, and 444 kg/mol, corresponding to bottlebrush N_{bb} of 37, 89, and 120, respectively (**Table 1**). SEC measurements for PEO bottlebrush samples were run using a lithium bromide/dimethylformamide (DMF) mixture (0.05 M LiBr) as the mobile phase with total molecular weights of 316, 688, and 952 kg/mol corresponding to N_{bb} of 85, 186, and 257, respectively (**Table 1**). The graft density (σ) of PS and PEO were calculated to be 0.037 and 0.025, respectively, using the bottlebrush molecular weight and the polymer mass fractions measured from thermogravimetric analysis (TGA) (see **Supporting Information**). The PDMS bottlebrush polymer molecular weight characterization was not accurately measured *via* SEC due to the HF cleaving process where HF will etch the silica particle and the PDMS side chain siloxane

bonds. Representative transmission electron microscopy (TEM) images of the polymer grafted particles are shown in **Figures 2e-g**.

Table 1. Molecular characterization of bottlebrushes after acid cleaving from silica particles.[a]

Sample[b]	Side Chain[c]			Backbone[c]			Graft Density[d]
	M_n (kg/mol)	$Đ_{sc}$	N_{sc}	M_n (kg/mol)	$Đ_{bb}$	N_{bb}	σ (# chains/nm^2)
PS-139	3.7	1.11	36	139	1.50	37	0.037
PS-327				327	1.49	89	
PS-444				444	1.52	120	
PDMS[e]	5.0*	N/A	67	N/A			N/A
PEO-316	3.7	1.03	84	316	1.44	85	0.025
PEO-688				688	1.26	186	
PEO-952				952	1.29	257	

[a]Silica particles are 160 nm in diameter. [b]PS, PDMS, and PEO are bottlebrush side chains, backbones are poly(norbornene). [c]Molecular weight characteristics were determined *via* SEC−MALS. [d]Graft density is calculated from M_n and TGA (see **Supporting Information**). [e]PDMS bottlebrushes could not be characterized due to polymer degradation during acid cleaving process. *Reported value from Gelest.

PGP Brush Height Influenced By Different Conditions

Brush heights of the bottlebrush PGPs were measured in solution and melt states. For solutions, dynamic light scattering (DLS) was used to obtain the hydrodynamic diameter of the PGPs. All three polymer chemistries showed increasing brush height with increasing backbone polymerization. The PS and PDMS samples were measured in THF with brushes increasing from 20, 57, to 83 nm for PS and 18, 48, to 103 nm for PDMS (**Figures 3a,c**). The PEO samples were measured in water with brushes increasing from 45, 87, to 168 nm (**Figures 3b**). To confirm hydrodynamic size increase was not the result of aggregating particles, the PEO bottlebrush PGPs were analyzed using cryogenic transmission electron microscopy (cryo-TEM). Images at lower magnification confirm the particles are not aggregating (see **Supporting Information**), while

higher magnifications show extended polymer chains "sticking out" from the particle surfaces (**Figures 3d-f**). Further, the measured brush heights from cryo-TEM increase from 35, 58, to 78 nm as N_{bb} increases. The trend is consistent with the DLS results and the slight discrepancy in values likely results from the overestimation of hydrodynamic size known to occur in DLS.[63] On the other hand, the cryo-TEM values may be underestimated as polymer density decreases further from the particle surface, and the image contrast decreases causing the polymer ends to "disappear".[64] Additionally, polymer degradation during cryo-TEM is not believed to be an issue as the dosage of 20 $e^-/Å^2$ was used and has been previously shown to not degrade biological samples.[65] With the PNBE backbone degree of polymerization increasing from 85 to 257 for the PEO bottlebrush samples, the brush heights increase from 30-50 nm to 80-170 nm. These results are comparable to fully extended bottlebrushes as measured by contour length of the poly(norbornene) backbone (see **Supporting Information**).

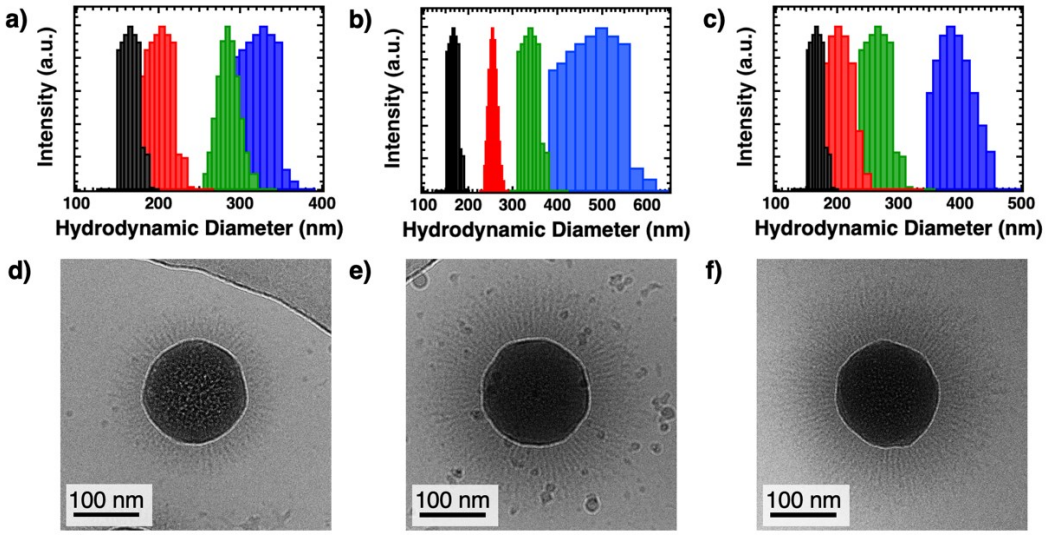

Figure 3. Characterization of bottlebrush PGP brush heights in solution. Hydrodynamic diameter size distributions measured using DLS of (a) PS, (b) PEO, and (c) PDMS PGPs with

norbornene functionalized particles (black) and bottlebrush PGPs with increasing N_{bb} (red, green, blue). Cryo-TEM micrographs of PEO samples with increasing N_{bb} (d) 85, (e) 186, and (f) 257.

Dissipative particle dynamics (DPD) simulations of the grafted bottlebrush conformations were conducted to confirm and interpret the experimental results. Grafting densities and chain lengths were selected to match the experimental values. In the simulations, the bottlebrushes were attached to a planar substrate to better represent the experimental system as the radius of gyration (R_g) for the bottlebrushes (e.g., 15 – 25 nm) is less than the radius of the 160 nm diameter silica particles. Thus, the local environment the bottlebrush experiences in the experiments is more representative of flat surface versus a curved one. A variety of work has been conducted to simulate the conformation of bottlebrushes on flat surfaces primarily based on graft density, showing the higher densities promote extended conformations while smaller brush heights occur at lower grafting, due to folding/bending of the bottlebrush backbones.[51,52]

In **Figure 4a**, representative snapshots from the DPD simulations show the differences between grafting linear polymers and bottlebrushes, with identical backbone (N_{bb}) or chain (N) lengths, to the same surfaces. The higher density of monomers for the bottlebrush architecture results in a larger brush height as compared to the grafted linear polymers. Similar to the TEM micrographs in **Figures 3d-f**, the simulations show that the bottlebrush backbones (red beads) are highly stretched at a grafting density of $\sigma = 0.04$ chains/$r_c^2 \approx 0.04$ chains/nm^2. The DPD simulations are quantified in **Figures 4b-c** which show the scaling of the root mean-squared radius of gyration and molecular shape anisotropy as a function of the polymer backbone length at two grafting densities of $\sigma \approx 0.02$ (open points) and 0.04 chains/nm^2 (closed points). **Figure 4b** compares the scaling of R_g for the bottlebrushes (circles) to the linear polymers (triangles) on a double logarithmic scale, showing a single scaling relation exists for each of the four brush

systems. Not only is R_g larger for the grafted bottlebrushes by a factor of ≈ 5, but the scaling exponents for the bottlebrush systems are larger than for the linear systems and increase as the grafting density increases from σ ≈ 0.02 to 0.04 chains/nm^2 from 0.77 to 0.81 (bottlebrush) and from 0.65 to 0.69 (linear). The degree to which the backbone is extended was quantified by computing the shape anisotropy, κ^2, from the gyration tensor. κ^2 takes on values between 0 (symmetric) and 1 (rigid rod). **Figure 4c** compares κ^2 for the grafted bottlebrushes to the linear polymers. As N_{bb} increases, κ^2 increases from below 0.2 to approximately 0.9 for N_{bb} = 120, indicating that the bottlebrush backbones are highly elongated, in good agreement with the experimental measurements in **Figure 3**. In contrast, as N increase for the linear polymers, κ^2 remains below 0.3 indicating that the polymers are largely symmetric.

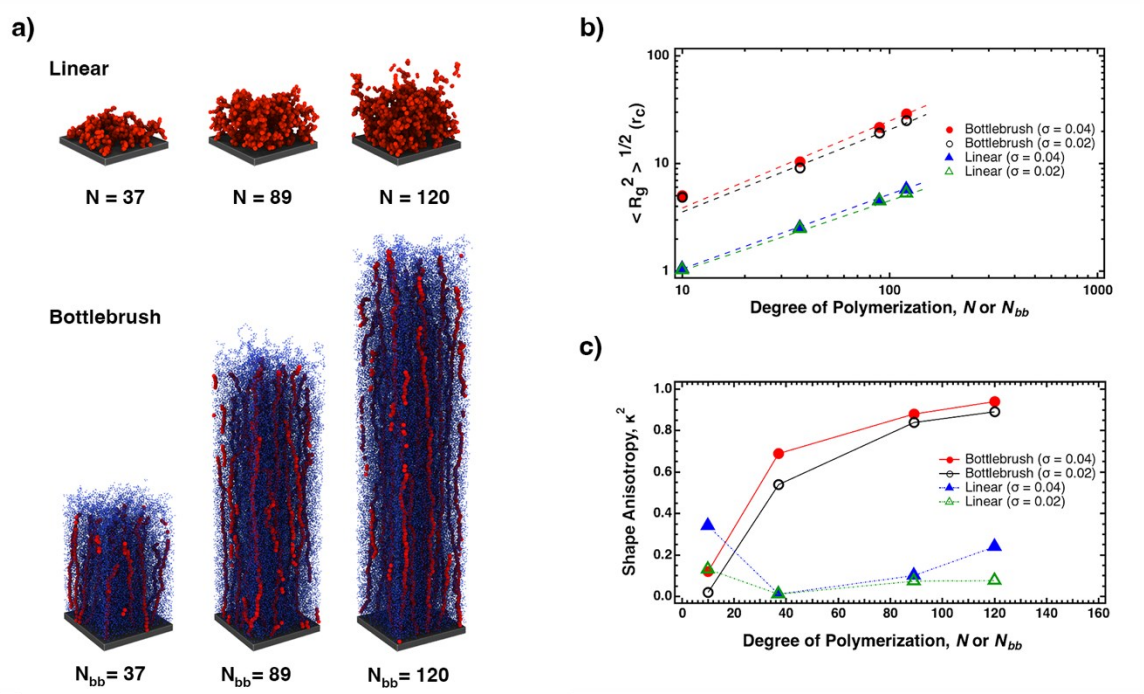

Figure 4. Computational analysis of PGP brush heights. (a) Snapshots of the brush for (top) linear homopolymers and (bottom) bottlebrushes at a grafting density of σ = 0.04 chains/r_c^2 ≈ 0.04 chains/nm^2. (b) Root mean-squared radius of gyration of the grafted polymers as a function of

backbone length for grafted bottlebrushes (circles) and linear polymers (triangles). Filled symbols correspond to a grafting density of $\sigma \approx 0.04$ chains/nm^2 and open symbols to $\sigma \approx 0.02$ chains/nm^2. (c) Shape anisotropy factor, κ^2, for the brushes. κ^2 is bounded between 0 for a symmetric molecule and 1 for a rigid rod (i.e., fully elongated).

In solution, PGP brush height increases linearly with N_{bb} suggesting a fully stretched chain, however, the brush height scaling in the melt state is drastically different. Melt state brush heights, or shell thickness, can be estimated using the known mass fractions and polymer density to obtain radius for the whole PGP. For example, PS samples with N_{bb} 37, 89, 120, were expected to have brush heights at 8, 15, 20 nm (see **Supporting Information**). This trend first appears to be consistent, albeit truncated, in the TEM results, in which the brush heights were calculated 5, 6, 12 nm with increasing N_{bb}. Brush heights were determined by measuring center-to-center interparticle distance in the TEM micrographs (**Figures 5a-c**), subtracting the particle diameter, and dividing by 2. However, each PS sample had a deviation of ± 5 or 6 nm, thus the brush heights are within error of each other, indicating no trend in particle spacing. The lack in particle spacing trend is indicated by the close packing of particles across all micrographs. The TEM samples were prepared by depositing PGP films on carbon grids *via* solution evaporation.[66] While the PS shells average 6 nm across N_{bb} samples, the PEO and PDMS samples averaged 3 and 1 nm, respectively (see **Supporting Information**). The close packing of particles is further demonstrated in ultra-small-angle X-ray scattering (USAXS) in which the three PS samples all display spherical form factors with the primary peaks at $q \approx 0.0040$ Å^{-1} (**Figure 5d**), and when accounting for pitch between layers, gives shell thicknesses of 17 nm (see **Supporting Information**). The non-trend

observed in the melt state measurements confirms the bottlebrushes are taking on a conformational state much different from those of the extended brushes in solution.

If the brushes were extended perpendicular to the particle surface while in the melt state, increasing interparticle distances would be expected. Thus, the consistency in interparticle distance across the N_{bb} range suggests the bottlebrush grafts collapse onto the particle surface. In the melt, the particles are in closer proximity, compared to the solution state, and therefore, strong interparticle interactions dominate, promoting the collapsed chain state.[67] Further, given the close packing of the particles, it is assumed the bottlebrushes occupy the interstitial spaces, resulting in non-uniform polymer shells. Therefore, the collapsed bottlebrushes may take on a spectrum of conformations from highly coiled to slightly stretched.

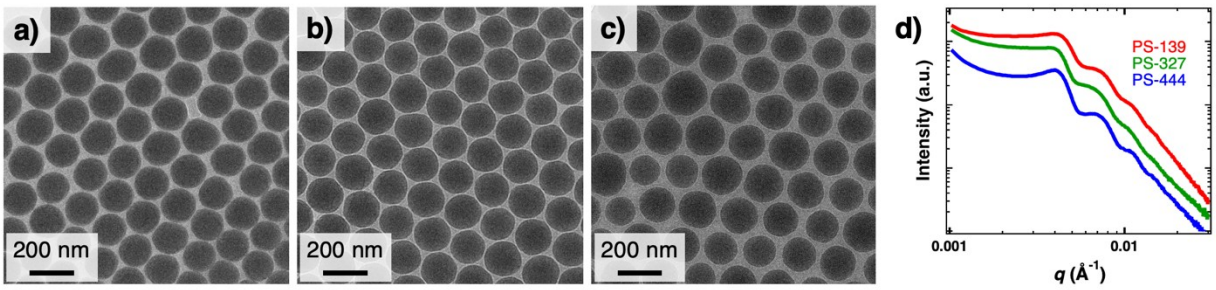

Figure 5. Bottlebrush PGP brush heights in the melt state. (a-c) TEM micrographs of PS PGPs with increasing N_{bb}. (d) USAXS of PS PGPs.

Impact of Polymer Conformation for PGPs with Non-Linear Architectures

Bottlebrush grafted nanoparticles offer a unique impact on PGP materials not seen with linear polymers due to the architectural diversity. As shown here, the bottlebrush polymer chains attached to "flat" surfaces undergo conformational extremes based on environmental conditions that do not occur with linear polymers (**Figure 6**). In the case of polymer grafted nanoparticles with linear

chains, there are two key brush regimes: the concentrated and semi-dilute (**Figure 6b**).[12,68] These regimes form as a function of free volume as controlled by polymer molecular weight, PGN graft density, volume fractions, and surface curvature. Bottlebrush PGPs studied here do not follow this trend, instead, two regimes, stretched and collapsed, form as a function of sample environmental conditions. In solution, brush height scales with N_{bb}, consistent with the backbone contour length, in contrast, in the melt, bottlebrushes collapse around particles, independent of N_{bb}, summarized for the PEO samples in **Figure 6a**.

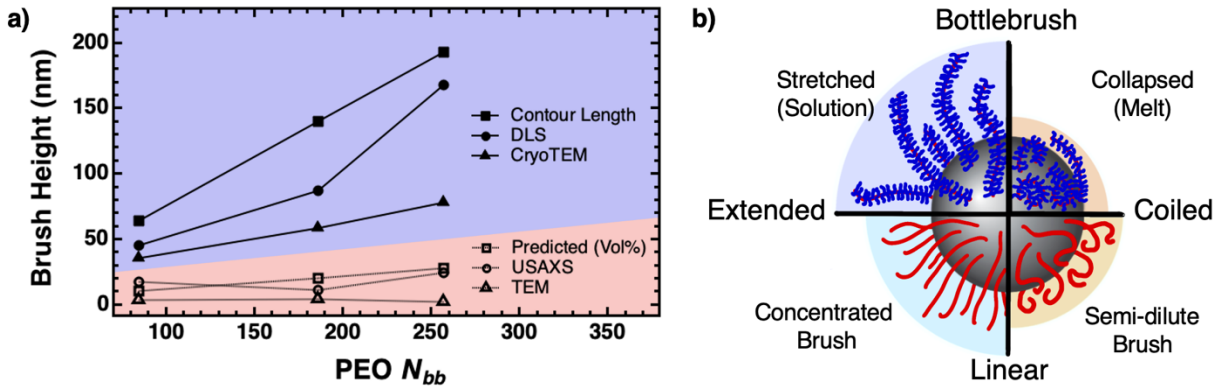

Figure 6. Macromolecular Architecture Impact on Polymer Brush Height. (a) Summary of PEO bottlebrush PGP brush heights as local environment changes. Blue background represents solvated conditions with contour length (filled square), DLS (filled circle), and CryoTEM (filled triangle) measurements. Red background represents melt state conditions with predicted height by volume fraction (open square), USAXS (open circle), and TEM (open triangle) measurements. (b) Scheme comparing different polymer brush regimes for bottlebrush and linear polymers.

In contrast to linear PGNs in the literature, the PGPs reported here have lower surface curvatures and polymer volume fractions. Therefore, we aimed to better replicate the conditions

of linear PGN brush regimes on higher curvature surfaces. To this end, PEO bottlebrush PGPs with varying N_{bb} were synthesized using the same SI-ROMP method previously described. These bottlebrushes were grafted from silica particles 77 ± 7 nm in diameter—about half the size of those discussed earlier. The same PEO macromonomer (M_n = 3.7 kg/mol) was used to produce two bottlebrush PGP samples with molecular weights of 183 and 649 kg/mol, corresponding to N_{bb} values of 49 and 175, respectively. Polymer fractions remained low, 33 and 56 vol%, and the graft density was 0.02 chains/nm^2. Brush heights were evaluated in the same manner as the larger particle samples (**Figure S8 and Table S9**). First, dynamic light scattering (DLS) of the PEO bottlebrush PGPs in water yielded brush heights of 57 and 281 nm. Cryo-TEM also indicated that the chains were protruding, with measured brush heights of 23 and 70 nm. Conventional TEM images of the smaller particle PEO bottlebrush PGPs showed brush heights of 3 and 4 nm. The results for 77 nm particle PGPs show increased brush heights in solution and minimal brush heights in the melt, consistent to what was reported for the larger 160 nm particles. Significant conformational changes due to environmental effects are consistent across the two different particle sizes and contrast sharply with the behavior seen in linear PGN systems reported in the literature.

However, even with 77 nm particle PGP studies, the linear PGN regimes and our system are not directly comparable. As mentioned, the larger particle sizes of the bottlebrush PGPs presented here are more representative of flat surfaces and have a higher volume fraction of particles. While our results for particles with 160 and 77 nm diameters are consistent, it is still unknown if the trends translate to smaller particles. The changes in bottlebrush polymer conformation when attached to even smaller particles (e.g., < 50 nm) has yet to be determined, but we suspect that higher curvature will prevent full chain collapse due to higher polymer volume

fractions. In the PGPs reported here, bottlebrush polymer volume fractions range from approximately 20-60%, while literature reports on linear cases show polymer fractions that are typically upwards of 90%.[8,9,12,68]

Regardless of curvature, it is intriguing how particles defy expectations of bottlebrush polymers, overcoming the drive for bottlebrush polymers to be preferentially stretched, allowing particles to tightly pack in the melt. This packing suggests that particle-particle interactions heavily influence chain conformations in the melt, superseding the bottlebrush's drive towards an extended conformation, likely resulting in a nonuniform polymer shell in which the bottlebrush conformations range from coiled to bent to stretched and occupy interstitial spaces between particles.

Although we cannot directly compare linear PGNs to the bottlebrush PGPs presented here, we highlight this comparison to underscore the relationship between polymer chain conformation and the resulting material properties, emphasizing that material design parameters for non-linear PGPs will be different from those developed by current methods. Polymer conformations and the resulting brush heights of linear PGNs have been widely studied as impacted by molecular weight, graft density, and surface/neighboring interactions.[69–74] The work reported here is the first of its kind to emphasize the connection between polymer chain conformation on the structure and properties of the material for nonlinear polymer grafted particle systems with experimental results.

Conclusion

Polymer grafted nanoparticles offer exciting possibilities to control nanoparticle dispersion within polymer matrices. The scope of previous work has been limited to linear polymer architectures. Here, we report that bottlebrush polymers grafted to particles exhibit drastically different chain conformational changes compared to grafted linear chains. The chain conformations span the extremes from fully stretched to collapsed when transitioned from a solvated state to the melt state. The reported results of the PGPs do not directly translate to linear PGN conformational regimes as the surface curvatures and polymer volume fractions are considerably lower. However, the findings are unique nonetheless, particularly in that they also defy expectations of bottlebrush conformations on flat surfaces with comparable graft density. Because the connection between graft chain conformation and a material's end-properties has been well established, ultimately, the work here supports an understanding of bottlebrush graft conformation that is yet to be reported.

Materials and Methods

Materials

Tetraethyl orthosilicate, ammonium hydroxide (28% in water), Grubbs' second-generation catalyst, 3-bromopyridine, pyridine, ethyl vinyl ether, hydrofluoric acid (49% aq.), deuterated chloroform, pentane, tetrahydrofuran, dimethylformamide dichloromethane, N,N′-dicyclohexylcarbodiimide, exo-5-norbornenecarboxylic acid, and 4-dimethylaminopyridine were purchased from Sigma-Aldrich. Poly(dimethyl siloxane) (monocarbinol terminated) and (5-Bicyclo[2.2.1]hept-2-enyl)triethoxysilane were purchased from Gelest. Ethanol, methanol, and diethyl ether were purchased from ThermoFisher Scientific. No purification or modification was performed unless stated otherwise.

Silica Particle Synthesis and Surface Functionalization

Silica particles are synthesized with Stöber processing, resulting in spherical particles ~160 nm in diameter.[62] First, 400 mL ethanol (EtOH) and 26 mL of ammonium hydroxide solution (NH4OH 28% in water) were added to a 1 L round bottom flask. Then, 12 mL tetraethylorthosilicate (TEOS) was added and the solution was mixed overnight at 500 rpm. The following morning, silica NP surfaces are functionalized with norbornenyltriethoxylsilane (NBES) by adding an additional 400 mL of EtOH and 2 mL NBES and refluxing at 70˚C overnight.[25] The particles are collected by distilling the mixture at 110˚C until approximately 300 mL remain, then purified *via* centrifugation to remove any unreacted reagents. The NP solutions are centrifuged at 10,000 rpm for 20 minutes then decanted and resuspended in tetrahydrofuran (THF). This process is repeated twice, and a final centrifugation at 2,500 rpm for 3 minutes is conducted to separate out any large aggregates.

The remaining product is stored in suspension in anhydrous THF at 3˚C, an aliquot is removed to determine product mass and concentration.

Grubbs' 3rd Generation Catalyst

Grubbs' 2nd generation catalyst (G2) was reacted with pyridine (10M excess) while stirring for 10 minutes. A red to green color change indicates the formation of Grubbs' 3rd generation catalyst (G3) which is precipitated in 10 mL of pentane, then filtered, vacuum dried, and stored under argon.[75]

Macromonomer Functionalization

Macromonomers with a norbornene end group were made after first collecting PS and PEO synthesized *via* in-house anionic polymerization[76] and PDMS commercially, all mono-hydroxyl terminated. Esterification reactions are conducted similar to previous reports,[77] in a glovebox 5-8 g polymer, N,N′-dicyclohexylcarbodiimide (DCC) (1:7), exo-5-norbornenecarboxylic acid (1:2), and 4-dimethylaminopyridine (1:0.4) were dissolved in 30-40 mL anhydrous dichloromethane. Solutions were stirred for 48 hours then filtered to remove DCC and precipitated in methanol (PS, PDMS) or diethyl ether (PEO) to collect polymer. Polymers were dissolved in tetrahydrofuran (THF) and precipitated 3 total times to remove impurities.

Surface Initiated Ring Opening Metathesis (SI-ROMP)

First, reaction vials are prepared in glovebox by dissolving norbornene functionalized macromonomer (100 mg to 1 g) in anhydrous THF (200 mg/mL). Next, the particles are activated in a glovebox by dissolving G3 (85mg) in anhydrous THF (2-3 mL) then adding silica particles

(1.5 g in THF). The particles stir in the catalyst solution for 15 minutes then 3BP (5 mL, 0.02 M in THF) is added and stirred for an additional minute. The G3 is added in excess to ensure complete activation of the NPs, however the excess must be removed to ensure polymerization only occurs from the particle surface (i.e. free homopolymer synthesis is limited). The 3BP is added to stabilize the catalyst during the purification of the activated particles (AP). The AP solution is centrifuged (11,000 rpm, 7 minutes) in a sealed tube then sonicated and vortexed in fresh THF (anhydrous, 0.02 M 3BP) three times. A light centrifugation (2,500 rpm, 3 minutes) separates out large aggregates and the remaining AP supernatant is added to the reaction vials (0.5 g each).[22] The reactions stir for 40 min at 40 ˚C then terminated with 2 mL ethyl vinyl ether to remove G3 from the polymer chains. Products are purified in THF *via* the centrifugation process used above, then stored in THF in a refrigerator.

Dynamic Light Scattering (DLS)

PGP solutions (1 mg/ml) are prepared in THF (PDMS, PS) or water (PEO) and filtered through 1 μm PTFE. DLS measurements are done using a Brookhaven Instruments BI-200SM Research goniometer system with a 637 nm, 30 mW laser, and a 100 μm aperture. The intensity autocorrelation function was recorded at room temperature for 4 measurements at each of 4 detector angles (45°, 60°, 90°, 120°) and the average was used for data analysis. The autocorrelation function was analyzed using the CONTIN algorithm to determine the average diffusion coefficient, and the hydrodynamic diameter of the diffusing particles was calculated using the Stokes−Einstein relation.

Thermogravimetric Analysis (TGA)

Measurements are performed on a TA Instruments Q600 using 5–10 mg of vacuum dried sample placed in alumina crucibles. Samples are initially held at 100 °C for 20 min remove any residual moisture then are heated to 800 °C at a rate of 10 °C/min. Overall polymer mass content is determined by evaluating mass loss between 100 °C and 800 °C.

Differential Scanning Calorimetry (DSC)

Thermal analysis of the PEO PGPs was conducted *via* TA Instrument Q2000 DSC. Samples (5-10 mg) in an aluminum pan followed a heat, cool, heat cycle up to 100 ºC, down to -60 ºC and back up to 100 ºC at 10 ºC/min with 5 min isotherms at each extreme. The reported traces show the second heating cycle.

Polymer Cleavage *via* Hydrofluoric Acid and Size-Exclusion Chromatography with Multi-Angle Light Scattering Detector (SEC-MALS)

Polymer-grafted particles (100–250 mg in THF) are dissolved in 20 mL of THF before being added to a PTFE dish. 10 drops (~1 mL) of HF (49% aq.) are added to the dish and allowed to evaporate overnight.[78] Once the HF has evaporated, recovered polymer is dried under vacuum. Cleaved polymer samples (5 mg/mL) are prepared and filtered with 0.45 μm PTFE filter prior to characterization. SEC measurements are conducted in THF (PS) or DMF (0.05M LiBr) (PEO) at 40˚C on a Tosoh EcoSEC equipped with a Wyatt Dawn Heleos-II eight angle light scattering detector. BI-DNDC refractometer was used to obtain dn/dc values of 0.203 (PS-NB BB in THF) and 0.038 (PEO-NB BB in DMF (0.05M LiBr)).

Transmission Electron Microscopy (TEM)

Micrographs are taken with a FEI Tecnai G2 Spirit BioTwin TEM. Silica particle samples are prepared by drop casting 1 mg/mL THF solutions on to carbon/copper 200 mesh grids. PGP samples are prepared by placing carbon/copper mesh grids in a vial then adding 300 μL of 2-3 mg/ml THF solutions. Samples produce self-assembled thin films through solvent evaporation overnight.[66] All grids are vacuum dried prior to imaging. Particle sizes are measured using ImageJ.

Cryo-TEM

For the 160 nm particles, samples were prepared by vitrifying 3 μL of 1 mg/mL PGP solutions on gold 300-mesh quantifoil grids (R2/1) using a Mark IV Vitrobot (Thermo Fisher) with the following parameters: Temperature = 4 ˚C, Humidity = 95%, Blot Time = 3.5 sec, Blot Force = 5. Grids were transported under LN and loaded into the Krios cryo-TEM equipped with a Bioquantum Energy Filter and K3 direct electron detector (Gatan). Projection images were collected at 4.6 Å/pixel with a total electron dose of 20 $e^-/Å^2$. For the 77 nm particles, samples were prepared by vitrifying 3 μL of 1 mg/mL solutions on copper 300-mesh quantifoil grids (R1.2/1.3) using a Mark IV Vitrobot (Thermo Fisher) with the following parameters: Temperature = 4°C, Humidity = 100%, Blot Time = 4 sec, Blot Force = -1. The grids were transported under LN and loaded into the FEI Titan Krios G3 equipped with Bioquantum Energy Filter, C_s image corrector, and Falcon 4 direct electron detector. The TEM micrographs were acquired at an accelerating voltage of 300 kV at 8.5 Å/pixel with a total electron dose of 18.5 $e^-/Å^2$.

USAXS

USAXS experiments were carried out on a Rigaku Smartlab with a Cu K alpha source at 44mA/40kV using the Bonse-Hard optics with a Ge(220) crystal at a scan resolution of 0.0001 degrees (2θ) and a scan speed of 0.0021 deg/min.

Simulation

Dissipative particle dynamics (DPD) simulations were performed using a GPU-accelerated, in-house code (gDPD). GPU acceleration was performed using the NVIDIA CUDA platform, and simulations were run on NVIDIA V100 GPUs. Simulations were performed under good solvent conditions, using identical parameters and methodology to a recent DPD study of bottlebrush polymers in solution.[79] To simulate grafted bottlebrushes, the leading monomer of the backbone was anchored to a planar substrate (thickness $h = 2\ r_c$) using a harmonic bond with a strength of $k_H = 50\ \epsilon_0/r_c^2$. The planar substrate was oriented parallel to the *xy*-plane, and created by arranging DPD particles into a face-centered cubic (FCC) lattice, and freezing their positions during the course of the simulation. Periodic boundary conditions were used in all directions with a system size of 24 x 24 x 192 r_c^3. To initialize the simulations, bottlebrushes were assigned a random grafting point on the substrate and left to equilibrate until their root mean-squared radius of gyration (R_g) reached a constant value, after which approximately 10^6 production time steps were performed to sufficiently sample the gyration tensor of the system. The mean-squared radius of gyration was calculated as the sum of the eigenvalues of the gyration tensor, *i.e.,* $R_g^2 = \lambda_1^2 + \lambda_2^2 + \lambda_3^2$, where $\lambda_1^2 \leq \lambda_2^2 \leq \lambda_3^2$. The shape anisotropy factor, κ^2, quantifies the degree to which the grafted polymers are preferentially extended along the eigenvector with the largest corresponding eigenvalue (i.e., λ_3^2). In our case, this eigenvector was essentially the *z*-axis. As with R_g, κ^2 is

defined from the eigenvalues of the gyration tensor as: $\kappa^2 = (3/2R_g^4)(\lambda_1^4 + \lambda_2^4 + \lambda_3^4) - 1/2$ and is bounded between 0 (isotropic) and 1 (perfectly aligned along the eigenvector corresponding to λ_3^2).

ASSOCIATED CONTENT

Supporting Information

Supporting information includes:

Polymer Elution via SEC

Polymer Mass Fraction and Graft Density via TGA

Polymer Brush Height Calculations

1D Scattering Plots of PGPs via USAXS

PGP Micrographs via TEM

PEO PGP Micrographs via CryoTEM

PEO PGP Crystallization via DSC

PEO PGPs with Small Particles

AUTHOR INFORMATION

Corresponding Author

Email: rjh64@psu.edu

ORCID

Robert J. Hickey: 0000-0001-6808-7411

Jensen N. Sevening: 0000-0002-1934-0617

Michael J. A. Hore: 0000-0003-2571-2111

Nehal Nupnar: 0009-0003-7103-3440

Soumyanil Adhikary: 0009-0009-5356-5041

Danielle Reifsnyder Hickey: 0000-0002-8962-1473

Notes

The authors declare no competing financial interest.

Acknowledgments

This work is supported by the National Science Foundation (NSF), Division of Materials Research Polymers Program (CAREER Proposal No.: DMR-1942508). TEM measurements (melt state) were taken at the Materials Characterization Lab (MCL) in the Materials Research Institute (MRI) at Penn State University. S.A. and D.R.H. acknowledge start-up funding from the Penn State Eberly College of Science, Department of Chemistry, College of Earth and Mineral Sciences, Department of Materials Science and Engineering, Materials Research Institute, and Huck Institutes of the Life Sciences. The co-authors acknowledge use of the Huck Institutes electron microscopy facilities and thank Sung Hyun Cho and Jessica L. Thompson for training and assistance on cryo-TEM and cryo-sample preparation.

References

(1) Winey, K. I.; Vaia, R. A. Polymer Nanocomposites. *MRS Bull* **2007**, *32*, 314–322. https://doi.org/10.1557/mrs2007.229.

(2) Bockstaller, M. R.; Mickiewicz, R. A.; Thomas, E. L. Block Copolymer Nanocomposites: Perspectives for Tailored Functional Materials. *Advanced Materials* **2005**, *17*, 1331–1349. https://doi.org/10.1002/adma.200500167.

(3) Nie, G.; Li, G.; Wang, L.; Zhang, X. Nanocomposites of Polymer Brush and Inorganic Nanoparticles: Preparation, Characterization and Application. *Polymer Chemistry* **2016**, 7(4), 753–769. https://doi.org/10.1039/c5py01333j.

(4) Bilchak, C. R.; Jhalaria, M.; Huang, Y.; Abbas, Z.; Midya, J.; Benedetti, F. M.; Parisi, D.; Egger, W.; Dickmann, M.; Minelli, M.; Doghieri, F.; Nikoubashman, A.; Durning, C. J.; Vlassopoulos, D.; Jestin, J.; Smith, Z. P.; Benicewicz, B. C.; Rubinstein, M.; Leibler, L.; Kumar, S. K. Tuning Selectivities in Gas Separation Membranes Based on Polymer-Grafted Nanoparticles. *ACS Nano* **2020**, *14* (12), 17174–17183. https://doi.org/10.1021/acsnano.0c07049.

(5) Yang, K.; Zhang, S.; He, J.; Nie, Z. Polymers and Inorganic Nanoparticles: A Winning Combination towards Assembled Nanostructures for Cancer Imaging and Therapy. *Nano Today* **2021**, 36, 101046. https://doi.org/10.1016/j.nantod.2020.101046.

(6) Pal, N.; Kumar, N.; Mandal, A. Stabilization of Dispersed Oil Droplets in Nanoemulsions by Synergistic Effects of the Gemini Surfactant, PHPA Polymer, and Silica Nanoparticle. *Langmuir* **2019**, *35* (7), 2655–2667. https://doi.org/10.1021/acs.langmuir.8b03364.

(7) Hooper, J. B.; Schweizer, K. S. Theory of Phase Separation in Polymer Nanocomposites. *Macromolecules* **2006**, *39* (15), 5133–5142. https://doi.org/10.1021/ma060577m.

(8) Kumar, S. K.; Jouault, N.; Benicewicz, B. C.; Neely, T. Nanocomposites with Polymer Grafted Nanoparticles. *Macromolecules* **2013**, *46* (9), 3199–3214. https://doi.org/10.1021/ma4001385.

(9) Yi, C.; Yang, Y.; Liu, B.; He, J.; Nie, Z. Polymer-Guided Assembly of Inorganic Nanoparticles. *Chem Soc Rev* **2020**, *49*, 465–508. https://doi.org/10.1039/C9CS00725C.

(10) Akcora, P.; Kumar, S. K.; Moll, J.; Lewis, S.; Schadler, L. S.; Li, Y.; Benicewicz, B. C.; Sandy, A.; Narayanan, S.; Ilavsky, J.; Thiyagarajan, P.; Colby, R. H.; Douglas, J. F. "Gel-like" Mechanical Reinforcement in Polymer Nanocomposite Melts. *Macromolecules* **2010**, *43* (2), 1003–1010. https://doi.org/10.1021/ma902072d.

(11) Chevigny, C.; Dalmas, F.; Di Cola, E.; Gigmes, D.; Bertin, D.; Boué, F.; Jestin, J. Polymer-Grafted-Nanoparticles Nanocomposites: Dispersion, Grafted Chain Conformation, and Rheological Behavior. *Macromolecules* **2010**, *44* (1), 122–133. https://doi.org/10.1021/ma101332s.

(12) Choi, J.; Hui, C. M.; Pietrasik, J.; Dong, H.; Matyjaszewski, K.; Bockstaller, M. R. Toughening Fragile Matter: Mechanical Properties of Particle Solids Assembled from Polymer-Grafted Hybrid Particles Synthesized by ATRP. *Soft Matter* **2012**, *8* (15), 4072–4082. https://doi.org/10.1039/c2sm06915f.

(13) Li, Y.; Tao, P.; Viswanath, A.; Benicewicz, B. C.; Schadler, L. S. Bimodal Surface Ligand Engineering: The Key to Tunable Nanocomposites. *Langmuir* **2012**, *29* (4), 1211–1220. https://doi.org/10.1021/la3036192.

(14) Gao, B.; Arya, G.; Tao, A. R. Self-Orienting Nanocubes for the Assembly of Plasmonic Nanojunctions. *Nat Nanotechnol* **2012**, *7* (7), 433–437. https://doi.org/10.1038/nnano.2012.83.
(15) Tawade, B. V.; Apata, I. E.; Pradhan, N.; Karim, A.; Raghavan, D. Recent Advances in the Synthesis of Polymer-Grafted Low-K and High-K Nanoparticles for Dielectric and Electronic Applications. *Molecules* **2021**, *26* (10), 2942–2986. https://doi.org/10.3390/molecules26102942.
(16) Feng, Y.; Ning, N.; Wei, Z.; Zhang, L.; Tian, M.; Zou, H.; Mi, J. Towards Optimization of Electrical Network and Mechanical Property of Polymer Nanocomposites with Grafted Nanoparticles. *Polymer* **2014**, *55* (14), 3178–3185. https://doi.org/10.1016/j.polymer.2014.05.012.
(17) Robbes, A.-S.; Cousin, F.; Meneau, F.; Dalmas, F.; Boué, F.; Jestin, J. Nanocomposite Materials with Controlled Anisotropic Reinforcement Triggered by Magnetic Self-Assembly. *Macromolecules* **2011**, *44* (22), 8858–8865. https://doi.org/10.1021/ma201096u.
(18) Fernandes, N. J.; Giannelis, E. P.; Koerner, H.; Vaia, R. A. Hairy Nanoparticle Assemblies as One-Component Functional Polymer Nanocomposites: Opportunities and Challenges. *MRS Commun* **2013**, *3* (1), 13–29. https://doi.org/DOI: 10.1557/mrc.2013.9.
(19) Ming Hui, C.; Pietrasik, J.; Schmitt, M.; Mahoney, C.; Choi, J.; Bockstaller, M. R.; Matyjaszewski, K. Surface-Initiated Polymerization as an Enabling Tool for Multifunctional (Nano-)Engineered Hybrid Materials. *Chemistry of Materials* **2013**, *26* (1), 745–762. https://doi.org/10.1021/cm4023634.
(20) Barbey, R.; Lavanant, L.; Paripovic, D.; Schüwer, N.; Sugnaux, C.; Tugulu, S.; Klok, H.-A. Polymer Brushes via Surface-Initiated Controlled Radical Polymerization: Synthesis, Characterization, Properties, and Applications. *Chem Rev* **2009**, *109* (11), 5437–5527. https://doi.org/10.1021/cr900045a.
(21) Akcora, P.; Liu, H.; Kumar, S. K.; Moll, J.; Li, Y.; Benicewicz, B. C.; Schadler, L. S.; Acehan, D.; Panagiotopoulos, A. Z.; Pryamitsyn, V.; Ganesan, V.; Ilavsky, J.; Thiyagarajan, P.; Colby, R. H.; Douglas, J. F. Anisotropic Self-Assembly of Spherical Polymer-Grafted Nanoparticles. *Nat Mater* **2009**, *8*, 354–359. https://doi.org/10.1038/NMAT2404.
(22) Lanasa, J. A.; Hickey, R. J. Surface-Initiated Ring-Opening Metathesis Polymerization: A Method for Synthesizing Polymer-Functionalized Nanoparticles Exhibiting Semicrystalline Properties and Diverse Macromolecular Architectures. *Macromolecules* **2020**, *53* (19), 8216–8232. https://doi.org/10.1021/acs.macromol.0c01381.
(23) Pribyl, J.; Benicewicz, B.; Bell, M.; Wagener, K.; Ning, X.; Schadler, L.; Jimenez, A.; Kumar, S. Polyethylene Grafted Silica Nanoparticles Prepared via Surface-Initiated ROMP. *ACS Macro Lett* **2019**, *8* (3), 228–232. https://doi.org/10.1021/acsmacrolett.8b00956.
(24) Zhu, T.; Anisur Rahman, M.; Benicewicz, B. C. Synthesis of Well-Defined Polyolefin Grafted SiO2 Nanoparticles with Molecular Weight and Graft Density Control. *ACS Macro Lett* **2020**, *9* (9), 1255–1260. https://doi.org/10.1021/acsmacrolett.0c00398.
(25) Anderson Jordi, M.; Seery, T. A. P. Quantitative Determination of the Chemical Composition of Silica−Poly(Norbornene) Nanocomposites. *J Am Chem Soc* **2005**, *127* (12), 4416–4422. https://doi.org/10.1021/ja044456i.

(26) Ning, X.; Jimenez, A. M.; Pribyl, J.; Li, S.; Benicewicz, B. C.; Kumar, S. K.; Schadler, L. S. Nanoparticle Organization by Growing Polyethylene Crystal Fronts. *ACS Macro Lett* **2019**, *8* (10), 1341–1346. https://doi.org/10.1021/acsmacrolett.9b00619.
(27) Bornani, K.; Anisur Rahman, M.; Benicewicz, B.; Kumar, S.; Schadler, L. Using Nanofiller Assemblies to Control the Crystallization Kinetics of High-Density Polyethylene. *Macromolecules* **2021**, *54* (12), 5673–5682. https://doi.org/10.1021/acs.macromol.1c00341.
(28) Sevening, J. N.; Dottin, S.; Torres, V. M.; Hickey, R. J. Soft Hybrid Elastomers Containing Polymer Grafted Nanoparticles. *Giant* **2022**, 12, 100133. https://doi.org/10.1016/j.giant.2022.100133.
(29) Radzinski, S. C.; Foster, J. C.; Scannelli, S. J.; Weaver, J. R.; Arrington, K. J.; Matson, J. B. Tapered Bottlebrush Polymers: Cone-Shaped Nanostructures by Sequential Addition of Macromonomers. *ACS Macro Lett* **2017**, *6* (10), 1175–1179. https://doi.org/10.1021/acsmacrolett.7b00724.
(30) Radzinski, S. C.; Foster, J. C.; Chapleski, R. C.; Troya, D.; Matson, J. B. Bottlebrush Polymer Synthesis by Ring-Opening Metathesis Polymerization: The Significance of the Anchor Group. *J Am Chem Soc* **2016**, *138* (22), 6998–7004. https://doi.org/10.1021/jacs.5b13317.
(31) Shieh, P.; Nguyen, H. V.-T.; Johnson, J. A. Tailored Silyl Ether Monomers Enable Backbone-Degradable Polynorbornene-Based Linear, Bottlebrush and Star Copolymers through ROMP. *Nat Chem* **2019**, *11* (12), 1124–1132. https://doi.org/10.1038/s41557-019-0352-4.
(32) Sheiko, S. S.; Sumerlin, B. S.; Matyjaszewski, K. Cylindrical Molecular Brushes: Synthesis, Characterization, and Properties. *Progress in Polymer Science* **2008**, 33, 759–785. https://doi.org/10.1016/j.progpolymsci.2008.05.001.
(33) Xie, G.; Martinez, M. R.; Olszewski, M.; Sheiko, S. S.; Matyjaszewski, K. Molecular Bottlebrushes as Novel Materials. *Biomacromolecules* **2019**, *20*, 27–54. https://doi.org/10.1021/acs.biomac.8b01171.
(34) Daniel, W. F. M.; Burdyńska, J.; Vatankhah-Varnoosfaderani, M.; Matyjaszewski, K.; Paturej, J.; Rubinstein, M.; Dobrynin, A. V; Sheiko, S. S. Solvent-Free, Supersoft and Superelastic Bottlebrush Melts and Networks. *Nat Mater* **2016**, *15* (2), 183–189. https://doi.org/10.1038/nmat4508.
(35) Keith, A. N.; Vatankhah-Varnosfaderani, M.; Clair, C.; Fahimipour, F.; Dashtimoghadam, E.; Lallam, A.; Sztucki, M.; Ivanov, D. A.; Liang, H.; Dobrynin, A. V; Sheiko, S. S. Bottlebrush Bridge between Soft Gels and Firm Tissues. *ACS Cent Sci* **2020**, *6*, 413–419. https://doi.org/10.1021/acscentsci.9b01216.
(36) Vashahi, F.; Martinez, M. R.; Dashtimoghadam, E.; Fahimipour, F.; Keith, A. N.; Bersenev, E. A.; Ivanov, D. A.; Zhulina, E. B.; Popryadukhin, P.; Matyjaszewski, K.; Vatankhah-Varnosfaderani, M.; Sheiko, S. S. Injectable Bottlebrush Hydrogels with Tissue-Mimetic Mechanical Properties. *Sci. Adv* **2022**, *8*, 2469. https://doi.org/10.1126/sciadv.abm2469
(37) Liberman-Martin, A. L.; Chu, C. K.; Grubbs, R. H. Application of Bottlebrush Block Copolymers as Photonic Crystals. *Macromol Rapid Commun* **2017**, *38*, 1700058. https://doi.org/10.1002/marc.201700058.

(38) Patel, B. B.; Walsh, D. J.; Kim, D. H.; Kwok, J.; Lee, B.; Guironnet, D.; Diao, Y. Tunable Structural Color of Bottlebrush Block Copolymers through Direct-Write 3D Printing from Solution. *Sci. Adv* **2020**, *6*, 7202–7212. https://doi.org/10.1126/sciadv.aaz7202
(39) Kim, N.-Y.; Moon, J.; Ryou, M.-H.; Kim, S.-H.; Kim, J.-H.; Kim, J.-M.; Bang, J.; Lee, S.-Y. Amphiphilic Bottlebrush Polymeric Binders for High-Mass-Loading Cathodes in Lithium-Ion Batteries. *Adv Energy Mater* **2022**, *12* (1), 2102109. https://doi.org/https://doi.org/10.1002/aenm.202102109.
(40) Jang, J.; Choi, C.; Kim, K.-W.; Okayama, Y.; Hyun Lee, J.; Read de Alaniz, J.; Bates, C. M.; Kon Kim, J. Triboelectric Nanogenerators: Enhancing Performance by Increasing the Charge-Generating Layer Compressibility. *ACS Macro Lett* **2022**, *11* (11), 1291–1297. https://doi.org/10.1021/acsmacrolett.2c00535.
(41) Karimkhani, V.; Vatankhah-Varnosfaderani, M.; Keith, A. N.; Dashtimoghadam, E.; Morgan, B. J.; Jacobs, M.; Dobrynin, A. V.; Sheiko, S. S. Tissue-Mimetic Dielectric Actuators: Free-Standing, Stable, and Solvent-Free. *ACS Appl Polym Mater* **2020**, *2* (5), 1741–1745. https://doi.org/10.1021/acsapm.0c00141.
(42) Nian, S.; Lian, H.; Gong, Z.; Zhernenkov, M.; Qin, J.; Cai, L.-H. Molecular Architecture Directs Linear–Bottlebrush–Linear Triblock Copolymers to Self-Assemble to Soft Reprocessable Elastomers. *ACS Macro Lett* **2019**, *8* (11), 1528–1534. https://doi.org/10.1021/acsmacrolett.9b00721.
(43) Grundler, J.; Shin, K.; Suh, H.-W.; Zhong, M.; Saltzman, W. M. Surface Topography of Polyethylene Glycol Shell Nanoparticles Formed from Bottlebrush Block Copolymers Controls Interactions with Proteins and Cells. *ACS Nano* **2021**, *15* (10), 16118–16129. https://doi.org/10.1021/acsnano.1c04835.
(44) Unsal, H.; Onbulak, S.; Calik, F.; Er-Rafik, M.; Schmutz, M.; Sanyal, A.; Rzayev, J. Interplay between Molecular Packing, Drug Loading, and Core Cross-Linking in Bottlebrush Copolymer Micelles. *Macromolecules* **2017**, *50* (4), 1342–1352. https://doi.org/10.1021/acs.macromol.6b02182.
(45) Fei, H. F.; Yavitt, B. M.; Nuguri, S.; Yu, Y. G.; Watkins, J. J. Ultrafast Self-Assembly of Bottlebrush Statistical Copolymers: Well-Ordered Nanostructures from One-Pot Polymerizations. *Macromolecules* **2021**, *54* (23), 10943–10950. https://doi.org/10.1021/acs.macromol.1c01311.
(46) Song, Q.; Dong, Q.; Liang, R.; Xue, Y.; Zhong, M.; Li, W. Hierarchical Self-Assembly of ABC-Type Bottlebrush Copolymers. *Macromolecules* **2023**, *56* (14), 5470–5481. https://doi.org/10.1021/acs.macromol.3c00440.
(47) Song, D. P.; Gai, Y.; Yavitt, B. M.; Ribbe, A.; Gido, S.; Watkins, J. J. Structural Diversity and Phase Behavior of Brush Block Copolymer Nanocomposites. *Macromolecules* **2016**, *49* (17), 6480–6488. https://doi.org/10.1021/acs.macromol.6b01602.
(48) Yavitt, B. M.; Fei, H. F.; Kopanati, G. N.; Winter, H. H.; Watkins, J. J. Liquid-to-Solid Transitions in Nanoparticle-Filled Brush Block Copolymer Composites. *Journal of Polymer Science* **2020**, *58* (22), 3227–3236. https://doi.org/10.1002/pol.20200523.
(49) Xue, Y.; Song, Q.; Liu, Y.; Smith, D.; Li, W.; Zhong, M. Hierarchically Structured Nanocomposites via Mixed-Graft Block Copolymer Templating: Achieving Controlled Nanostructure and Functionality. *J Am Chem Soc* **2023**, *146, 567-577.* https://doi.org/10.1021/jacs.3c10297.
(50) Modica, K. J.; Martin, T. B.; Jayaraman, A. Effect of Polymer Architecture on the Structure and Interactions of Polymer Grafted Particles: Theory and Simulations.

Macromolecules **2017**, *50* (12), 4854–4866. https://doi.org/10.1021/acs.macromol.7b00524.
(51) Leuty, G. M.; Tsige, M.; Grest, G. S.; Rubinstein, M. Tension Amplification in Tethered Layers of Bottle-Brush Polymers. *Macromolecules* **2016**, *49* (5), 1950–1960. https://doi.org/10.1021/acs.macromol.5b02305.
(52) Jungmann, P.; Kreer, T.; Sommer, J.-U.; Paturej, J. Conformational Properties of End-Grafted Bottlebrush Polymers. *Macromolecules* **2021**, *54* (1), 161–169. https://doi.org/10.1021/acs.macromol.0c01586.
(53) Wernersson, E.; Linse, P. Spreading and Brush Formation by End-Grafted Bottle-Brush Polymers with Adsorbing Side Chains. *Langmuir* **2013**, *29* (33), 10455–10462. https://doi.org/10.1021/la4021959.
(54) Cao, Q.; Zuo, C.; Ma, Y.; Li, L.; Chen, S.; Hu, Z. Molecular Dynamics Simulations of End-Grafted Polymers with Charged Side Chains. *J Polym Sci B Polym Phys* **2011**, *49* (12), 882–889. https://doi.org/10.1002/polb.22257.
(55) Verduzco, R.; Li, X.; Pesek, S. L.; Stein, G. E. Structure, Function, Self-Assembly, and Applications of Bottlebrush Copolymers. *Chem. Soc. Rev* **2015**, *44*, 2405. https://doi.org/10.1039/c4cs00329b.
(56) Jiang, L.; Nykypanchuk, D.; Pastore, V. J.; Rzayev, J. Morphological Behavior of Compositionally Gradient Polystyrene–Polylactide Bottlebrush Copolymers. *Macromolecules* **2019**, *52* (21), 8217–8226. https://doi.org/10.1021/acs.macromol.9b01756.
(57) Lu, Z.-Q.; Yin, Z.; Zhang, L.-L.; Yan, Y.; Jiang, Z.; Wu, H.; Wang, W. Synthesis of Proton Conductive Copolymers of Inorganic Polyacid Cluster Polyelectrolytes and PEO Bottlebrush Polymers. *Macromolecules* **2022**, *55* (8), 3301–3310. https://doi.org/10.1021/acs.macromol.1c02443.
(58) Erabhoina, H.; Rosenbach, D.; Mohanraj, J.; Thelakkat, M. Solid Polymer Nanocomposite Electrolytes with Improved Interface Properties towards Lithium Metal Battery Application at Room Temperature. *Electrochim Acta* **2021**, *387, 138455*. https://doi.org/10.1016/j.electacta.2021.138455.
(59) Burdyńska, J.; Daniel, W.; Li, Y.; Robertson, B.; S. Sheiko, S.; Matyjaszewski, K. Molecular Bottlebrushes with Bimodal Length Distribution of Side Chains. *Macromolecules* **2015**, *48* (14), 4813–4822. https://doi.org/10.1021/acs.macromol.5b00795.
(60) Liang, H.; Morgan, B. J.; Xie, G.; Martinez, M. R.; Zhulina, E. B.; Matyjaszewski, K.; Sheiko, S. S.; Dobrynin, A. V. Universality of the Entanglement Plateau Modulus of Comb and Bottlebrush Polymer Melts. *Macromolecules* **2018**, *51* (23), 10028–10039. https://doi.org/10.1021/acs.macromol.8b01761.
(61) Lin, T.-P.; Chang, A. B.; Lennon Luo, S.-X.; Chen, H.-Y.; Lee, B.; Grubbs, R. H. Effects of Grafting Density on Block Polymer Self-Assembly: From Linear to Bottlebrush. *ACS Nano* **2017**, *11* (11), 11632–11641. https://doi.org/10.1021/acsnano.7b06664.
(62) Ohno, K.; Morinaga, T.; Koh, K.; Tsujii, Y.; Fukuda, T. Synthesis of Monodisperse Silica Particles Coated with Well-Defined, High-Density Polymer Brushes by Surface-Initiated Atom Transfer Radical Polymerization. *Macromolecules* **2005**, *38*, 2137–2142. https://doi.org/10.1021/ma048011q.

(63) Li, Y.; Lubchenko, V.; Vekilov, P. G. The Use of Dynamic Light Scattering and Brownian Microscopy to Characterize Protein Aggregation. *Review of Scientific Instruments* **2011**, *82* (5), 053106. https://doi.org/10.1063/1.3592581.
(64) Wittemann, A.; Drechsler, M.; Talmon, Y.; Ballauff, M. High Elongation of Polyelectrolyte Chains in the Osmotic Limit of Spherical Polyelectrolyte Brushes: A Study by Cryogenic Transmission Electron Microscopy. *J Am Chem Soc* **2005**, *127* (27), 9688–9689. https://doi.org/10.1021/ja0513234.
(65) Taylor, K. A.; Glaeser, R. M. Electron Microscopy of Frozen Hydrated Biological Specimens. *J Ultrastruct Res* **1976**, *55*, 448–456. https://doi.org/10.1016/S0022-5320(76)80099-8.
(66) Bodnarchuk, M. I.; Kovalenko, M. V.; Heiss, W.; Talapin, D. V. Energetic and Entropic Contributions to Self-Assembly of Binary Nanocrystal Superlattices: Temperature as the Structure-Directing Factor. *J Am Chem Soc* **2010**, *132* (34), 11967–11977. https://doi.org/10.1021/ja103083q.
(67) Koerner, H.; Drummy, L. F.; Benicewicz, B.; Li, Y.; Vaia, R. A. Nonisotropic Self-Organization of Single-Component Hairy Nanoparticle Assemblies. *ACS Macro Lett* **2013**, *2* (8), 670–676. https://doi.org/10.1021/mz4001805.
(68) Jiao, Y.; Tibbits, A.; Gillman, A.; Hsiao, M.-S.; Buskohl, P.; Drummy, L. F.; Vaia, R. A. Deformation Behavior of Polystyrene-Grafted Nanoparticle Assemblies with Low Grafting Density. *Macromolecules* **2018**, *51*, 7257. https://doi.org/10.1021/acs.macromol.8b01524.
(69) Wu, Z.; Pal, S.; Keten, S. Implicit Chain Particle Model for Polymer-Grafted Nanoparticles. *Macromolecules* **2023**, *56* (9), 3259–3271. https://doi.org/10.1021/acs.macromol.2c02272.
(70) Ethier, J. G.; Hall, L. M. Modeling Individual and Pairs of Adsorbed Polymer-Grafted Nanoparticles: Structure and Entanglements. *Soft Matter* **2018**, *14* (4), 643–652. https://doi.org/10.1039/c7sm02116j.
(71) Ethier, J. G.; Hall, L. M. Structure and Entanglement Network of Model Polymer-Grafted Nanoparticle Monolayers. *Macromolecules* **2018**, *51* (23), 9878–9889. https://doi.org/10.1021/acs.macromol.8b01373.
(72) Yuan, C.; Käfer, F.; Ober, C. K. Polymer-Grafted Nanoparticles (PGNs) with Adjustable Graft-Density and Interparticle Hydrogen Bonding Interaction. *Macromol Rapid Commun* **2022**, *43* (12), 2100629. https://doi.org/10.1002/marc.202100629.
(73) Cang, Y.; Reuss, A. N.; Lee, J.; Yan, J.; Zhang, J.; Alonso-Redondo, E.; Sainidou, R.; Rembert, P.; Matyjaszewski, K.; Bockstaller, M. R.; Fytas, G. Thermomechanical Properties and Glass Dynamics of Polymer-Tethered Colloidal Particles and Films. *Macromolecules* **2017**, *50* (21), 8658–8669. https://doi.org/10.1021/acs.macromol.7b01752.
(74) Choi, J.; Hore, M. J. A.; Clarke, N.; Winey, K. I.; Composto, R. J. Nanoparticle Brush Architecture Controls Polymer Diffusion in Nanocomposites. *Macromolecules* **2014**, *47* (7), 2404–2410. https://doi.org/10.1021/ma500235v.
(75) Love, J. A.; Morgan, J. P.; Trnka, T. M.; Grubbs, R. H. A Practical and Highly Active Ruthenium-Based Catalyst That Effects the Cross Metathesis of Acrylonitrile. *Angewandte Chemie* **2002**, *114* (21), 4207–4209. https://doi.org/10.1002/1521-3773(20021104)41:21<4035::AID-ANIE4035>3.0.CO;2-I

(76) Lang, C.; Lanasa, J. A.; Utomo, N.; Xu, Y.; Nelson, M. J.; Song, W.; Hickner, M. A.; Colby, R. H.; Kumar, M.; Hickey, R. J. Solvent-Non-Solvent Rapid-Injection for Preparing Nanostructured Materials from Micelles to Hydrogels. *Nat Commun* **2019**, *10*, 3855. https://doi.org/10.1038/s41467-019-11804-7.
(77) Fei, H.; Yavitt, B. M.; Kopanati, G.; Watkins, J. J. Effect of Side Chain and Backbone Length on Lamellar Spacing in Polystyrene-Block-Poly(Dimethyl Siloxane) Brush Block Copolymers. *J Polym Sci, Part B: Polym Phys* **2019**, 57, 691-699. https://doi.org/10.1002/polb.24824.
(78) Chancellor, A. J.; Seymour, B. T.; Zhao, B. Characterizing Polymer-Grafted Nanoparticles: From Basic Defining Parameters to Behavior in Solvents and Self-Assembled Structures. *Anal Chem* **2019**, *91* (10), 6391–6402. https://doi.org/10.1021/acs.analchem.9b00707.
(79) Mukkamala, R. S.; Hore, M. J. A. Simulation and Analysis of Molecular Bottlebrush Dynamics in Dilute Solutions. *Macromolecules* **2024**, *57* (2), 445–455. https://doi.org/10.1021/acs.macromol.3c02259.